Increased cochlear otic capsule thickness and intracortical canal porosity in the *oim* mouse model of osteogenesis imperfecta

Running title: 3D morphology of the *oim* otic capsule and cochlea

Authors: Annalisa De Paolis[1], Brendyn James Miller[2], Michael Doube[3], Andrew John Bodey[4], Christoph Rau[4,5,6], Claus-Peter Richter[5,7,8], Luis Cardoso[1], Alessandra Carriero[1]

Affiliations:

[1] Department of Biomedical Engineering, The City College of New York, New York, NY, USA

[2] Department of Bioengineering, Clemson University, Clemson, SC

[3] Department of Infectious Diseases and Public Health, City University of Hong Kong, HK

[4] Diamond Light Source, Harwell Science and Innovation Campus, Didcot, UK

[5] Department of Otolaryngology, Northwestern University Feinberg School of Medicine, Chicago, IL, USA

[6] University of Manchester, Manchester, UK

[7] Department of Biomedical Engineering, Northwestern University, Evanston, IL, USA

[8] The Hugh Knowles Center, Department of Communication Sciences and Disorders, Northwestern University, Evanston, IL, USA

Corresponding Author: Dr. Alessandra Carriero
Department of Biomedical Engineering
The City College of New York
160 Convent Avenue, Steinman Bldg. room 403C
New York, NY10031
email: acarriero@ccny.cuny.edu
tel: +1 212 650 7591

Number of tables: 2

Number of figures: 3

Supplemental material: 4 Figures and 3 Tables

Declarations of interest: none

Abstract

Osteogenesis imperfecta (OI or *brittle bone disease*) is a group of genetic disorders of the connective tissues caused mainly by mutations in the genes encoding collagen type I. Clinical manifestations of OI include skeletal fragility, bone deformities, and severe functional disabilities, such as hearing loss. Progressive hearing loss, usually beginning in childhood, affects approximately 70% of people with OI with more than half of the cases involving the inner ear. There is no cure for OI nor a treatment to ameliorate its corresponding hearing loss, and very little is known about the properties of OI ears. In this study, we investigate the morphology of the otic capsule and the cochlea in the inner ear of the *oim* mouse model of OI. High-resolution 3D images of 8-week old *oim* and WT inner ears were acquired using synchrotron microtomography. Volumetric morphometric measurements were conducted for the otic capsule, its intracortical canal network and osteocyte lacunae, and for the cochlear spiral ducts. Our results show that the morphology of the cochlea is preserved in the *oim* ears at 8 weeks of age but the otic capsule has a greater cortical thickness and altered intracortical bone porosity, with a larger number and volume density of highly branched canals in the *oim* otic capsule. These results portray a state of compromised bone quality in the otic capsule of the *oim* mice that may contribute to their hearing loss.

Keywords: osteogenesis imperfecta, *oim*, cochlea, otic capsule, cortical bone, porosity

Introduction

Osteogenesis imperfecta (OI or *brittle bone disease*) is a heritable bone disease caused mainly by mutations of collagen type I, the primary matrix protein in the human body [1-4]. As a consequence of these mutations, the collagen molecules are improperly folded in the OI connective tissues, the fibril alignment and tissue structure are disrupted, and an abnormal template is provided for mineralization in the bone matrix [5, 6]. Clinical manifestations of OI are extreme skeletal fragility, decreased bone mineral density, bone deformities and severe functional disabilities, such as cardiac deficiency, restrictive pulmonary disorders and hearing loss [7-9].

Approximately 70% of people with OI experience progressive hearing loss [10-15], with 11-31% of cases happening in children under 9 years old [12, 16-21] and in 15-94% in children up to 19 years of age [10-12, 17-20, 22, 23]. More than half of the hearing loss cases in OI are sensorineural, occurring either independently or simultaneously alongside conductive hearing loss [10-15]. To date, little is known about the mechanisms leading to the onset and progression of hearing loss in OI, and there is no cure for OI nor a treatment to ameliorate its corresponding hearing loss. Analyses of OI ears displayed signs of abnormal bone growth, increased cortical bone porosity, and lesions, already at a very young age (0-9 years old) [24-26]. The most affected areas include the otic capsule [24, 25, 27], the stapediovestibular joint [27-31], the oval and round window, and the internal auditory canal [24, 25, 30, 32, 33]. In some cases, the organ of Corti and spiral ganglion neurons showed deterioration with spiral ligament hyalinization and stria vascularis atrophy [28, 30, 34, 35]. Other people with OI exhibited new bone formation in the scala tympani and endolymphatic duct surrounded by thicker and highly porous bone [24, 25, 30, 32, 33]. Previous studies have associated

polymorphisms in the COL1A1 regulatory regions with abnormal bone in people with OI [36, 37] as well as in other adult populations [38, 39]. A recent study found that conductive but not sensorineural or mixed hearing loss has been associated with lower total bone tissue mass (areal BMD) in people with OI [40]. Due to the difficulties in conducting a comprehensive investigation of hearing loss in living people with OI, a corresponding mouse model of OI hearing loss would allow studying the pathogenic mechanisms underlying auditory dysfunction in OI. However, to date, there have been just a few studies completed. Preliminary observations conducted on Mov-13 mice, a mouse model of mild OI (type I), showed that hearing loss began at 15 weeks of age and was associated with fibrosis and fixation of the stapes footplate but not with active abnormal otic capsule remodeling [41, 42]. More recently, a preliminary study conducted on 2-8 ears of a Prolyl 3-hydroxylase-1 null (P3H1) mouse model of recessive OI found elevated auditory thresholds and abnormal morphology of their middle ear ossicles [43]. Finally, auditory impairments were experienced by the homozygotes B6C3Fe-a/aCol1a2$^{oim/oim}$ (*oim*) mouse model of severe OI and the authors suggested it had to be related to the abnormal expression and formation of Col1α1 homotrimers in this mouse model [38]. However, while the hearing loss is documented in the OI mice, the mechanisms for their hearing loss are unknown. This study therefore examines the inner ear morphology of the homozygotes *oim* mice, to provide novel insights into the properties of the *oim* ear and the mechanisms leading to hearing loss.

The *oim* mouse model has been extensively used to study OI, its collagenous tissues, and the effect of therapies for bone fragility because it mimics the biochemical and phenotypic features of the most debilitating, non-lethal human forms of OI. Homozygous *oim* mice have small body and head size [44, 45], severe osteopenia, bone fragility, multiple fractures,

impaired growth [44], lower bone formation rate [46], matrix abnormalities [47-50], altered long bone intracortical canal and lacunar porosity [51], less stiff collagen fibril and bone tissue matrix, and disorganized lamellar structures that contribute to its brittleness [52]. Since the *oim* mouse suffers from hearing loss [38], it is of paramount importance to fully understand the role of micromorphology in the maintenance of ear integrity and function in these mice. Changes in the cochlear architecture, otic capsule morphology and its intracortical porosity are critical in determining the mechanical properties of the inner ear [53-57] and may have consequent adverse effects on the bone conduction [40, 58-60] as well as on the cochlear function of transferring pressure waves [61, 62] and transducing them into electrical signals [63, 64]. This study, therefore, examines the 3D cochlear and otic capsule morphology and inner ear intracortical bone tissue properties in the homozygotes *oim* mouse model of OI using synchrotron microtomography. Our future studies will investigate changes in the *oim* mouse middle ear and in the soft tissues in the cochlea, as well as the relative contributions to hearing loss from the middle and inner ear.

Material and Methods

Sample Preparation and Data Collection

The bullae of fresh frozen 8-week old male *oim* (B6C3Fe-a/a-Col1a2$^{oim/oim}$) and WT (B6C3Fe-a/a-Col1a2$^{+/+}$) mice (N = 6/group) were dissected. The long bones of these same mice were previously used in other studies [52, 65]. Before imaging at the synchrotron, the bullae were aligned and wrapped in gauze with physiological saline solution, and stored at -20 ºC. Synchrotron X-ray microtomography was conducted at the Diamond-Manchester Imaging Branchline I13-2 [66, 67] of Diamond Light Source, UK. A partially-coherent, filtered, polychromatic 'pink' beam (8 to 30 keV) of parallel geometry was generated by an

undulator of 5 mm gap, and used to image the cochlea and otic capsule of each mouse ear. For each scan, 3001 projection images of 400 ms exposure time were acquired at equally-spaced angles over 180° of continuous rotation around the cochlea's longitudinal axis. The last projection was compared to the first to check for possible sample deformation, bulk movements and radiation damages. Images were collected by a pco.edge 5.5 Camera Link detector (PCO AG, Germany) mounted on a visible-light microscope of variable magnification. Magnification was controlled via rotation of a turret incorporating various scintillator-coupled objective lenses. A 4 × objective, coupled to a 750 μm $CdWO_4$ scintillator, mounted ahead of a 2 × lens provided 8 × total magnification, a field of view of 2.1 × 1.8 mm (2560 × 2160 pixels) and an effective pixel size of 0.8125 μm. A propagation distance of approximately 5 mm was used to provide minimal inline phase contrast. Before the reconstruction via filtered back projection with DAWN 1.7 [68], projection images were flat and dark-field corrected and ring artifact suppression was performed [69]. The morphology of the otic capsule cortical bone and the cochlear fluid compartments was then assessed.

Otic capsule morphology

For each sample, the original stack of images was histogram normalized in ImageJ [70] and imported in DataViewer (v.1.5.1.2, Skyscan, Belgium) to be reoriented in the three-dimensional space. The rotated images were binned with a factor of 5 and loaded into Mimics Research (v.21, Materialise, Leuven, Belgium) to be segmented for air, soft and calcified tissues using an automated thresholding algorithm [61]. Masks representing the 3D volume of cortical bone, soft tissue, auditory nerve and cochlear fluid scalae were created. Since the Reissner's membrane was not observed, scala vestibuli and scala media were combined for

the following morphometrical analysis. The otic capsule cortical thickness was measured on the coronal and sagittal planes at their intersection with the cochlear modiolus (Fig. S1A) and on two transverse planes crossing the middle and apical turn of the cochlea (Fig. S1B), using CTAn (v. 1.14.4.1, Skyscan, Belgium) after manual segmentation of the cortical bone from the surrounding trabecular bone and soft tissue. De-speckling and morphological operations were performed to digitally remove the intracortical porosity and noise before the calculation of the average cortical thickness (Fig. 1). Measurements were reported for the averaged thickness of the otic capsule on the coronal (Oc.Th.cor), sagittal (Oc.Th.sag) and transverse planes in the middle (Oc.Th.tra.M) and apical (Oc.Th.tra.A) turns. The otic capsule length in the coronal plane (Oc.Le) was also measured (Fig. S1C).

3D morphologic analysis of the otic capsule intracortical bone porosity, i.e. canals and osteocyte lacunae, was conducted by using the 'Particle Analyser' routine in BoneJ [71] on the original thresholded (histogram-based global algorithm in ImageJ) images to segment the bone matrix from the air and soft tissue [51]. Furthermore, individual intracortical canals from branched networks were analyzed using the 'Skeletonize 3D' and the 'Analyse Skeleton' functions in BoneJ [71]. At the tissue level, we analyzed cortical bone volume (Ct.TV), cortical bone porosity (Po.V/Ct.TV), canal number (N.Ca), canal number density (N.Ca/Ct.TV), canal volume density (Ca.V/Ct.TV), canal connectivity density (Ca.Conn.D), mean canal volume (<Ca.V>), mean canal diameter (<Ca.D>) and mean canal length (<Ca.Le>). At the cellular level, the number of osteocyte lacunae (N.Lc), lacuna number density (N.Lc/Ct.TV), lacuna volume density (Lc.V/Ct.TV), mean lacuna volume (<Lc.V>), mean lacuna equancy, elongation and flatness (<Lc.Eq>, <Lc.El>, <Lc.Fl>, respectively) and mean lacuna orientation (<Lc.θ>) were examined [51].

Cochlear morphology

Cochlear gross-dimensions were estimated from the 3D rendering of the scala tympani, and the combined scala vestibuli and media from the above segmentation in Mimics Research and after consistent alignment of the renderings in the 3D space. The total volume of the scalae (Sc.Fl.V), the volume of the final segment of the apical turn (Sc.Fl.Tip.V) (Fig. S2), and the cochlear external spiral length (Sc.Fl.Sp.Le) were quantified for each sample (Fig. S3A-B) together with the surfaces and the perimeters of the fluid scalae on the coronal and sagittal planes, as selected above (Fig. S2B and Fig. 2A-B). Furthermore, the pitch of the middle (Sc.Fl.Pitch.tra.M) and the apical (Sc.Fl.Pitch.tra.A) turn of the cochlear spiral were measured on the coronal plane (Fig. S3C), while the maximum axis of the fluid scalae was evaluated along the coronal (Sc.Fl.corAxis.tra.M and Sc.Fl.corAxis.tra.A) and sagittal direction (Sc.Fl.sagAxis.tra.M and Sc.Fl.sagAxis.tra.A) on the two aforementioned planes (Fig. S4).

Bone tissue mineral density of the otic capsule

For assessment of the degree of mineralization of the otic capsule, differences in the gray color intensity of the scans was analyzed. First, the dynamic range of the original 32-bits stack of images was downsized to 8-bits. The stack of images was standardized using the "normalize" procedure in ImageJ [70] with a 1% saturation factor. Images were imported into Matlab (v.2020 MathWorks) to compute the histogram of gray color representing X-Ray attenuation of air, soft and mineralized tissues. The histogram of each sample was normalized by the amplitude and standard deviation of the peak representing Air. The stack of images was then imported into CTAnalyzer (v. 1.14.4.1, Skyscan, Belgium), and the degree of mineralization was determined for each sample. Degree of mineralization is reported in

arbitrary units (A.U.) since the histograms of gray color intensity were normalized to the peak representing air in each scan.

Statistical analyses

Statistical differences between the *oim* and WT bone properties (having the same number of samples within the two groups) were evaluated by performing the Student's independent *t*-test for the variables that were normally distributed, while the Mann-Whitney rank test was used to evaluate variables with non-normal distributions. Mean properties of canal and lacunae derived from samples of different size were evaluated with multilevel linear models, which accounted for the hierarchical dependence of the sample from the specific bone within each group, and the maximum likelihood was assessed to estimate the overall fit of the data to the model. Variables with *p*-values less than 0.05 were considered to be statistically significant. The effect size (Cohen's *d*) on the morphological parameters was calculated for each variable to determine the magnitude of the observed effect.

Results

Otic capsule morphology

Morphological assessment of the otic capsule thickness and length and its intracortical porosity in 8-week old *oim* and WT mice using synchrotron microtomography is reported in Table 1. We observed an increased cortical bone thickness in the coronal plane (Oc.Th.cor, $p<0.05$ - Table 1) in the *oim* otic capsule with no major statistically significant difference in the length at the whole organ level.

Morphometric evaluation of WT and *oim* otic capsule at the tissue and cellular scale length (Fig. 3A-B) indicated a greater intracortical bone porosity in *oim* mice (Po.V/Ct.TV, Table

1, $p<0.05$). Morphological measurements of intracortical bone porosity at the tissue level (Table 1), indicates that the *oim* otic capsule has larger number and higher volume density of canals (N.Ca/Ct.TV and Ca.V/Ct.TV, $p<0.05$), which are extremely interconnected to each other (Ca.Conn.D, $p<0.05$). Intracortical canals here include both the blood vessels and possible resorption voids. 3D reconstructions of the canal network presented in Figure 3C show that the *oim* otic capsule exhibits numerous branched and interconnected canals, many more than in WT bone. No differences in the mean canal volume, diameter or length between *oim* and WT cochlear bone were observed. At the cellular level, no differences between genotypes were observed in the lacuna number, volume and density, and in the mean lacuna shape and orientation (Table 1).

Cochlear morphology

Morphometric analysis of WT and *oim* cochlear fluid scalae (Fig. S2), cochlear spiral length and pitch of the middle and apical turn (Fig. S3), major cochlear axis length (Fig. S4), and scalae perimeter and surface area (Fig. 2A-B) resulted in non-significant differences between the two groups of mice (Table 2 and Fig. 2C-D).

The effect size on the morphological parameters

Morphological parameters, such as otic capsule thickness, coronal maximum axis of the fluid scalae at the apical turn, and fluid scalae tip volume and area, had a large variance relative to the effect size in our cohort of mice. Results from a one-sided beta/type-II error test ($\alpha = 0.05$, power = 0.80 conducted on the non-significant parameters to determine the sample size - Tables S1-S3) indicate the tendency of the *oim* inner ear to have a thicker cortex in the transverse plane at the apical and middle turns, with a shorter maximum axis of the fluid

scalae at the apical turn, and a smaller tip of the cochlear fluid scalae, if a sample size of 12-25 were to be considered in each group.

Bone tissue mineral density of the otic capsule

The mean and standard deviation of the histogram peak representing the degree of mineralization was 171.60±4.05 and 173.80±12.77 A.U. for the WT and *oim* groups, respectively. The mean degree of mineralization value of the *oim* group is slightly higher than that of the WT group, and the standard deviation of the *oim* showed a much larger variability than the standard deviation observed in the WT group. A paired t-test between these two groups has a $p > 0.05$, indicating that no statistically significant differences between genotypes were observed in the degree of mineralization of their otic capsules at 8 weeks of age.

Discussion

This study quantitatively investigates the 3D morphology of the cochlea and otic capsule of 8-week old *oim* mice using images collected with synchrotron microtomography. Increased cortical thickness in the coronal plane and altered intracortical vascular porosity with more numerous, densely packed and highly branched canals were observed in the *oim* otic capsule. Variation in the otic capsule thickness in the absence of notable changes in the cochlear fluid scalae between *oim* and WT ears at 8 weeks of age is in agreement with previous histological findings from a 9 years old child with OI type III [30] and an infant with OI type II [72] that reported a thicker temporal bone with normal cochlea morphology. Also, CT scans of the temporal bones in young adults (19-36 years old) with OI showed a thicker otic capsule [26, 73, 74]. At the tissue level, the increased intracortical bone porosity we found in the *oim* otic

capsule due to more abundant, more densely packed and highly interconnected canals is comparable with those from CT and MRI studies conducted on human inner ears reporting higher canal porosity in the otic capsule of people with OI [75-77]. This confirms that the *oim* mouse model has similar morphological changes as in humans with OI. Understanding the changes in the *oim* ear morphology helps to better understand OI disease in which deafness is an important sequela. The morphological changes here observed in the otic capsule of the *oim* mice, and particularly the increased tissue porosity may contribute to the hearing loss of the *oim* mice by 1) directly reducing bone conduction; and/or 2) increasing the formation of microcracks in the otic capsule, which may in turn affect bone conduction and/or cochlear fluid flow; and/or 3) altering the cochlea blood flow regulation, which in turn affects the ion and fluid balance in the inner ear and the function of the sensory hair cells.

The *oim* cochlear otic capsule cortical thickness is about 14.3% higher than in the WT counterparts with no changes in TMD. This is a remarkable variation for the *oim* mice cochlear otic capsule, particularly considering that the *oim* mice have reduced body mass and smaller head size with shorter nasal bones, compared to WT mice [45]. *Oim* long bones are shorter and more gracile (with a smaller diameter and thinner cortex) than WT counterparts [44]. Interestingly, the *oim* inner ear have same cochlear volume as in WT mice inner ears, but a thicker cortex of the otic capsule in the coronal plane, which may be related to the shorter proportional rostral-caudal skull length of the *oim* mice [45]. Furthermore, the *oim* otic capsule has increased intracortical porosity with altered geometry. It is unknow yet if these changes are associated with hearing loss reducing bone conduction or if they are instead a compensatory effect in an attempt to maintain the hearing function. Future studies will need

to assess if the current configuration contributes to hearing loss in OI and if it is maintained with growth and aging in these mice.

Microcracks in the otic capsule have been reported for about a century now, and from the very beginning, they have been described as containing cellular connective tissue [78]. Their locations are consistent in the otic capsule [53, 56, 78, 79], and masticatory stresses have been proposed as the possible causes of these fatigue microcracks that form in the otic capsule [53]. Higher intracortical canal porosity has been previously associated with reduced fracture toughness in bone [80]. Our previous studies have shown that many intracortical canals highly connected to each other, like those observed in the *oim* otic capsule, can produce high strain and stress concentrations within the bone therefore increasing crack initiation and propagation within the bone [51, 52, 65]. Therefore, the changes in the otic capsule intracortical architecture may easily increase the number of microfractures (or microfissures) and fatigue microdamage, that normally form in the otic capsule during growth, thus causing hearing loss in OI by adversely affecting the otic capsule mechanical integrity and increasing its fracture risk [53-56].

Finally, the changes in the otic capsule morphology may affect the mechanical integrity of the cochlea and thus affect hearing. Inner ear function depends both on its anatomy and on the material properties of its soft and hard tissues. Therefore, the increased intracortical porosity morphology of the *oim* otic capsule may alter the regulation of blood flow in the cochlear vasculature, resulting in vascular-related hearing impairment. Normal blood supply to the cochlea and blood labyrinth barrier is important for maintaining the endocochlear potential, ion transport, and endolymphatic fluid balance, and for avoiding cochlear toxicity from external substances [81]. Vascular barrier disruption in the stria vascularis affects the

ionic composition of endolymph and leads to reduction or loss of the endocochlear potential, resulting in hearing loss. Also, the structural change of the intracortical porosity in specific locations along the cochlear spiral could negatively affect the perception of definite frequencies given the tonotopic organization of the basilar membrane in the mammal cochlea [82, 83]. It is also possible that the ear collagenous soft tissues of windows and membranes are altered in the *oim* mice, further affecting the transmission of sound in their inner ears [84]. Our future studies will investigate the presence of hard and soft tissues and their material properties to determine the biomechanics of the inner ear mechanics in *oim* mice and define the relation between otic capsule changes and the sensorineural hearing loss in these mice.

In this study, we have found that osteocyte lacunae have similar densities and geometries in the *oim* and WT otic capsule cortical bone. The lack of changes in the lacuna configuration in the *oim* otic capsule is not surprising in the light of the findings of a recent study on MMP13 deficient mice with suppressed perilacunar remodeling, which reported no difference in lacuna number density nor in the mean lacunae volume in the cochlear otic capsule [85]. Also, the cochlear bone was able to maintain bone mass and bone quality independent of the presence of MMP13 [85]. This suggests that cellular mechanisms necessary for perilacunar remodeling are down-regulated in the cochlear bone, and that the mechanisms controlling bone remodeling in the otic capsule are different from those in the long bones, with the remodeling of the otic capsule bone happening at a very slow rate, perhaps to preserve the hearing function [85]. In support of these claims, an investigation on Mov-13 mouse has provided evidence that osteocytes of the otic capsule differ from osteocytes in long bone (tibia), even with Mov-13 otic capsule not exhibiting bone growth

abnormalities observed instead in human cases of OI type I [42]. To help explain the mechanisms of hearing loss in OI, further studies are needed to examine how the *oim* otic capsule bone thickness and intracortical porosity vary with development and growth in relation to their cellular activity and bone remodeling, and auditory function in the inner ear. There is also a need to establish the onset and progression of hearing loss in *oim* mice and the relative contribution of the middle ear (with collagenous tympanic membrane, ligaments and middle ear ossicles) and inner ear (with collagenous oval and round windows, basilar and tectorial membranes, and otic capsule) to the hearing loss reported in the *oim* mice [38]. Future studies will further need to establish whether the sensorineural hearing loss in the *oim* mice relates to impairments of the mechanotransduction process due to changes in mechanical properties of the collagenous tissues or if it is due to biochemical atrophy of the hair cells and stria vascularis.

Conclusions

Synchrotron microtomography revealed increased otic capsule thickness and intracortical porosity in the *oim* inner ear, with more numerous and highly connected canals than in WT. These results are in good agreement with the changes observed in the inner ear morphology observed in humans with OI associated hearing loss. Defects in the intracortical bone porosity and architecture may change the mechanical properties of the otic capsule, having deleterious implications for the cochlea's mechanical integrity and its ability to transmit vibrations to the hair cells stereocilia via bone conduction. A comprehensive understanding of how the cochlea and the surrounding otic capsule influence the auditory system in OI will provide further insights into the disease and guide the development of targeted treatments to halt or reduce its hearing loss.

Acknowledgments

This work was supported by the Diamond Light Source (MT9860) and the National Science Foundation (CBET-1829310).

CRediT author statement

Annalisa De Paolis: Methodology, Software, Formal analysis, Data curation, Writing-Original draft preparation, Writing – Review & Editing, Visualization. **Brendyn Miller:** Methodology, Software, Formal analysis, Data curation, Writing – Review & Editing, Visualization. **Micheal Doube:** Investigation, Software, Writing – Review & Editing. **Andrew John Bodey:** Investigation, Writing – Review & Editing. **Christoph Rau:** Investigation, Writing – Review & Editing. **Claus-Peter Richter:** Conceptualization, Writing – Review & Editing. **Luis Cardoso:** Conceptualization, Resources, Writing – Review & Editing. **Alessandra Carriero:** Conceptualization, Methodology, Investigation, Resources, Writing-Original draft preparation, Writing – Review & Editing, Visualization, Supervision, Project Administration, Funding acquisition.

References

1. Hartikka, H., et al., *Lack of correlation between the type of COL1A1 or COL1A2 mutation and hearing loss in osteogenesis imperfecta patients.* Hum Mutat, 2004. **24**(2): p. 147-54.
2. Marini, J. and S.M. Smith, *Osteogenesis Imperfecta*, in *Endotext*, K.R. Feingold, et al., Editors. 2000: South Dartmouth (MA).
3. Marini, J.C., et al., *Osteogenesis imperfecta.* Nat Rev Dis Primers, 2017. **3**: p. 17052.
4. Sillence, D.O., A. Senn, and D.M. Danks, *Genetic heterogeneity in osteogenesis imperfecta.* J Med Genet, 1979. **16**(2): p. 101-16.
5. Cole, W.G., *Advances in osteogenesis imperfecta.* Clin Orthop Relat Res, 2002(401): p. 6-16.
6. Cole, W.G., *The Nicholas Andry Award-1996. The molecular pathology of osteogenesis imperfecta.* Clin Orthop Relat Res, 1997(343): p. 235-48.
7. Kuurila, K., et al., *Hearing loss in children with osteogenesis imperfecta.* Eur J Pediatr, 2000. **159**(7): p. 515-9.
8. Paterson, C.R., E.A. Monk, and S.J. McAllion, *How common is hearing impairment in osteogenesis imperfecta?* J Laryngol Otol, 2001. **115**(4): p. 280-2.
9. Steiner, R.D. and D. Basel, *COL1A1/2 Osteogenesis Imperfecta*, in *GeneReviews((R))*, M.P. Adam, et al., Editors. 1993: Seattle (WA).
10. Stewart, E.J. and B.F. O'Reilly, *A clinical and audiological investigation of osteogenesis imperfecta.* Clin Otolaryngol Allied Sci, 1989. **14**(6): p. 509-14.
11. Pillion, J.P. and J. Shapiro, *Audiological findings in osteogenesis imperfecta.* J Am Acad Audiol, 2008. **19**(8): p. 595-601.
12. Pedersen, U., *Hearing loss in patients with osteogenesis imperfecta. A clinical and audiological study of 201 patients.* Scand Audiol, 1984. **13**(2): p. 67-74.
13. Kuurila, K., et al., *Hearing loss in Finnish adults with osteogenesis imperfecta: a nationwide survey.* Ann Otol Rhinol Laryngol, 2002. **111**(10): p. 939-46.
14. Hartikka, H., et al., *Lack of correlation between the type of COL1A1 or COL1A2 mutation and hearing loss in osteogenesis imperfecta patients.* Hum Mutat, 2004. **24**(2): p. 147-54.
15. Swinnen, F.K., et al., *Osteogenesis Imperfecta: the audiological phenotype lacks correlation with the genotype.* Orphanet J Rare Dis, 2011. **6**: p. 88.
16. Bergstrom, L., *Osteogenesis imperfecta:otological and maxillofacial aspects*. 1977, Laryngoscope. p. 1-42.
17. Cox, J.R. and C.L. Simmons, *Osteogenesis imperfecta and associated hearing loss in five kindreds.* South Med J, 1982. **75**(10): p. 1222-6.
18. Garretsen, T.J. and C.W. Cremers, *Clinical and genetic aspects in autosomal dominant inherited osteogenesis imperfecta type I.* Ann N Y Acad Sci, 1991. **630**: p. 240-8.
19. Garretsen, A.J., C.W. Cremers, and P.L. Huygén, *Hearing loss (in nonoperated ears) in relation to age in osteogenesis imperfecta type I.* Ann Otol Rhinol Laryngol, 1997. **106**(7 Pt 1): p. 575-82.
20. da Costa Otavio, A.C., et al., *Osteogenesis imperfecta and hearing loss: an analysis of patients attended at a benchmark treatment center in southern Brazil.* Eur Arch Otorhinolaryngol, 2020. **277**(4): p. 1005-1012.

21. Ting, T.H. and M.R. Zacharin, *Hearing in bisphosphonate-treated children with osteogenesis imperfecta: our experience in thirty six young patients.* Clin Otolaryngol, 2012. **37**(3): p. 229-33.
22. Imani, P., S. Vijayasekaran, and F. Lannigan, *Is it necessary to screen for hearing loss in the paediatric population with osteogenesis imperfecta?* Clin Otolaryngol Allied Sci, 2003. **28**(3): p. 199-202.
23. Riedner, E.D., L.S. Levin, and M.J. Holliday, *Hearing patterns in dominant osteogenesis imperfecta.* Arch Otolaryngol, 1980. **106**(12): p. 737-40.
24. Sando, I., et al., *Osteogenesis imperfecta tarda and otosclerosis. A temporal bone histopathology report.* Ann Otol Rhinol Laryngol, 1981. **90**(3 Pt 1): p. 199-203.
25. Nager, G.T., *Osteogenesis imperfecta of the temporal bone and its relation to otosclerosis.* Ann Otol Rhinol Laryngol, 1988. **97**(6 Pt 1): p. 585-93.
26. Sakai, O., et al., *Otosclerosis and Dysplasias of the Temporal Bone*, in *Head and Neck Imaging*, P.M. Som and H.D. Curtin, Editors. 2003, Mosby: S. Louis. p. 1245-1273.
27. Bretlau, P. and M.B. Jorgensen, *Otosclerosis and osteogenesis imperfecta.* Arch Otolaryngol, 1969. **90**(1): p. 4-10.
28. Swinnen, F.K., et al., *Audiometric, surgical, and genetic findings in 15 ears of patients with osteogenesis imperfecta.* Laryngoscope, 2009. **119**(6): p. 1171-9.
29. Pedersen, U., et al., *Histopathology of the stapes in osteogenesis imperfecta.* J Laryngol Otol, 1985. **99**(5): p. 451-8.
30. Santos, F., et al., *Otopathology in Osteogenesis Imperfecta.* Otol Neurotol, 2012. **33**(9): p. 1562-6.
31. Pillion, J.P., D. Vernick, and J. Shapiro, *Hearing loss in osteogenesis imperfecta: characteristics and treatment considerations.* Genet Res Int, 2011. **2011**: p. 983942.
32. Bretlau, P. and M. Balsley-Jorgensen, *Otosclerosis and osteogenesis imperfecta.* Acta Otolaryngol, 1969. **67**(2): p. 269-76.
33. Berger, G., et al., *Histopathology of the temporal bone in osteogenesis imperfecta congenita: a report of 5 cases.* Laryngoscope, 1985. **95**(2): p. 193-9.
34. Langman, A.W., R.K. Jackler, and F.A. Sooy, *Stapedectomy: Long-TErm Hearing Results*. 1991, Laryngoscope. p. 810-4.
35. Bergstrom, L., *Fragile bones and fragile ears.* Clin Orthop Relat Res, 1981(159): p. 58-63.
36. McKenna, M.J., et al., *Association of COL1A1 and otosclerosis: evidence for a shared genetic etiology with mild osteogenesis imperfecta.* Am J Otol, 1998. **19**(5): p. 604-10.
37. McKenna, M.J., A.G. Kristiansen, and A.S. Tropitzsch, *Similar COL1A1 expression in fibroblasts from some patients with clinical otosclerosis and those with type I osteogenesis imperfecta.* Ann Otol Rhinol Laryngol, 2002. **111**(2): p. 184-9.
38. Chen, W., et al., *Single-nucleotide polymorphisms in the COL1A1 regulatory regions are associated with otosclerosis.* Clin Genet, 2007. **71**(5): p. 406-14.
39. Khalfallah, A., et al., *Association of COL1A1 and TGFB1 polymorphisms with otosclerosis in a Tunisian population.* Ann Hum Genet, 2011. **75**(5): p. 598-604.
40. Swinnen, F.K., et al., *Association between bone mineral density and hearing loss in osteogenesis imperfecta.* Laryngoscope, 2012. **122**(2): p. 401-8.

41. Altschuler, R.A., et al., *An evaluation of otopathology in the MOV-13 transgenic mutant mouse.* Ann N Y Acad Sci, 1991. **630**: p. 249-52.
42. Stankovic, K.M., et al., *Studies of otic capsule morphology and gene expression in the Mov13 mouse--an animal model of type I osteogenesis imperfecta.* Audiol Neurootol, 2007. **12**(5): p. 334-43.
43. Pokidysheva, E., et al., *Prolyl 3-hydroxylase-1 null mice exhibit hearing impairment and abnormal morphology of the middle ear bone joints.* Matrix Biol, 2013. **32**(1): p. 39-44.
44. Chipman, S.D., et al., *Defective pro alpha 2(I) collagen synthesis in a recessive mutation in mice: a model of human osteogenesis imperfecta.* Proc Natl Acad Sci U S A, 1993. **90**(5): p. 1701-5.
45. Menegaz, R.A., S.H. Ladd, and J.M. Organ, *Craniofacial allometry in the OIM.* FASEB J, 2020. **34**(8): p. 10850-10859.
46. Kalajzic, I., et al., *Osteoblastic response to the defective matrix in the osteogenesis imperfecta murine (oim) mouse.* Endocrinology, 2002. **143**(5): p. 1594-601.
47. Camacho, N.P., et al., *The material basis for reduced mechanical properties in oim mice bones.* J Bone Miner Res, 1999. **14**(2): p. 264-72.
48. Phillips, C.L., et al., *Oim mice exhibit altered femur and incisor mineral composition and decreased bone mineral density.* Bone, 2000. **27**(2): p. 219-26.
49. Camacho, N.P., W.J. Landis, and A.L. Boskey, *Mineral changes in a mouse model of osteogenesis imperfecta detected by Fourier transform infrared microscopy.* Connect Tissue Res, 1996. **35**(1-4): p. 259-65.
50. Grabner, B., et al., *Age- and genotype-dependence of bone material properties in the osteogenesis imperfecta murine model (oim).* Bone, 2001. **29**(5): p. 453-7.
51. Carriero, A., et al., *Altered lacunar and vascular porosity in osteogenesis imperfecta mouse bone as revealed by synchrotron tomography contributes to bone fragility.* Bone, 2014. **61**: p. 116-24.
52. Carriero, A., et al., *How tough is brittle bone? Investigating osteogenesis imperfecta in mouse bone.* J Bone Miner Res, 2014. **29**(6): p. 1392-401.
53. Proops, D.W., W.M. Hawke, and G. Berger, *Microfractures of the otic capsule. The possible role of masticatory stress.* J Laryngol Otol, 1986. **100**(7): p. 749-58.
54. Frisch, T., et al., *Volume-referent bone turnover estimated from the interlabel area fraction after sequential labeling.* Bone, 1998. **22**(6): p. 677-82.
55. Frisch, T., et al., *Estimation of volume referent bone turnover in the otic capsule after sequential point labeling.* Ann Otol Rhinol Laryngol, 2000. **109**(1): p. 33-9.
56. Frisch, T., P. Bretlau, and M.S. Sorensen, *Intravital microlesions in the human otic capsule. Detection, classification and pathogenetic significance revisited.* ORL J Otorhinolaryngol Relat Spec, 2008. **70**(3): p. 195-201.
57. Frisch, T., et al., *Prevalence, size and distribution of microdamage in the human otic capsule*. 2015, Acta Oto-Laryngologica. p. 771-775.
58. Gargeshwari, A., et al., *Effect of Lowered Bone Mineral Density on the Outcomes of Audiological Tests: A Preliminary Study* 2017, J Indian Speech Language Hearing Assoc. p. 29-35.
59. Handoko, E., M.D. Murdiyo, and H. Soesanto, *The difference of otic capsule density, auditory ossicles density, and hearing threshold in osteoporosis and non-*

osteoporosis patients at Saiful Anwar Public Hospital 2017. 2018, Bali Med J. p. Bali Medical Journal (Bali Med J) 2018, Volume 7, Number 3: 764-768.
60. Yueniwati, Y. and Rosa, *The Significant Correlation Between the Density of the Cochlea Otic Capsule and Spine in Hearing Loss Patients.* Indian J Otolaryngol Head Neck Surg, 2019. **71**(Suppl 2): p. 1163-1168.
61. De Paolis, A., et al., *Human cochlear hydrodynamics: A high-resolution μCT-based finite element study.* J Biomech, 2017. **50**: p. 209-216.
62. De Paolis, A., et al., *Analytical and numerical modeling of the hearing system: Advances towards the assessment of hearing damage.* Hear Res, 2017. **349**: p. 111-128.
63. Ciganović, N., A. Wolde-Kidan, and T. Reichenbach, *Hair bundles of cochlear outer hair cells are shaped to minimize their fluid-dynamic resistance.* Sci Rep, 2017. **7**(1): p. 3609.
64. Zagadou, B., P. Barbone, and D.C. Mountain, *Significance of the Microfluidic Flow Inside the Organ of Corti.* J Biomech Eng, 2020.
65. Carriero, A., et al., *A methodology for the investigation of toughness and crack propagation in mouse bone.* J Mech Behav Biomed Mater, 2014. **39**: p. 38-47.
66. Pešić , Z.D., et al. *Experimental stations at I13 beamline at Diamond Light Source*. in *J. Phys.: Conf. Ser.* 2013.
67. Rau, C., et al., *Coherent imaging at the Diamond beamline I13.* Phys. Status Solidi A, 2011. **208**(11): p. 2522–2525.
68. Basham, M., et al., *Data Analysis WorkbeNch (DAWN).* J Synchrotron Radiat, 2015. **22**(3): p. 853-8.
69. Titarenko, V., *Analytical formula for two-dimensional ring artefact suppression.* J Synchrotron Radiat, 2016. **23**(Pt 6): p. 1447-1461.
70. Schneider, C.A., W.S. Rasband, and K.W. Eliceiri, *NIH Image to ImageJ: 25 years of image analysis.* Nat Methods, 2012. **9**(7): p. 671-5.
71. Doube, M., et al., *BoneJ: Free and extensible bone image analysis in ImageJ.* Bone, 2010. **47**(6): p. 1076-9.
72. Vianna, M.F., et al., *Temporal Bone Histopathology Case of the Month. Osteogenesis Imperfecta-A Human Temporal Bone Case Study*. 2013, Otology & Neurotology. p. e113-e114.
73. Tabor, E.K., et al., *Osteogenesis Imperfecta Tarda: Appearance of the Temporal Bones at CT*. 1990. p. 181-183.
74. L., H.T., D.D.M. Lin, and D.M. Yousem, *Case 48: Osteogenesis Imperfecta of the Temporal Bone*. 2002, Radiology. p. 166-170.
75. Marion, M.S. and R. Hinojosa, *Osteogenesis imperfecta.* Am J Otolaryngol, 1993. **14**(2): p. 137-8.
76. Alkadhi, H., D. Rissmann, and S.S. Kollias, *Osteogenesis imperfecta of the temporal bone: CT and MR imaging in Van der Hoeve-de Kleyn syndrome.* AJNR Am J Neuroradiol, 2004. **25**(6): p. 1106-9.
77. Hermie, I., M. Horvath, and S. Van Cauter, *Temporal Bone Imaging Features in Osteogenesis Imperfecta.* J Belg Soc Radiol, 2017. **101**(1): p. 27.
78. Mayer, O., *Die Ursache der Knochenneubildung bei der Otosklerose.* Acta Oto-Laryngologica, 1931. **15**(2-4): p. 407-408.

79. Hansen, L.J., et al., *Microcrack surface density in the human otic capsule: An unbiased stereological quantification.* Anat Rec (Hoboken), 2020.
80. Yeni, Y.N., et al., *The influence of bone morphology on fracture toughness of the human femur and tibia*. 1997, Bone. p. 453-59.
81. Shi, X., *Physiopathology of the cochlear microcirculation.* Hear Res, 2011. **282**(1-2): p. 10-24.
82. Zhang, X. and R.Z. Gan, *A comprehensive model of human ear for analysis of implantable hearing devices.* IEEE Trans Biomed Eng, 2011. **58**(10): p. 3024-7.
83. Gan, R.Z., B.P. Reeves, and X. Wang, *Modeling of sound transmission from ear canal to cochlea.* Ann Biomed Eng, 2007. **35**(12): p. 2180-95.
84. Zagadou, B.F., P.E. Barbone, and D.C. Mountain, *Elastic properties of organ of Corti tissues from point-stiffness measurement and inverse analysis.* J Biomech, 2014. **47**(6): p. 1270-7.
85. Jáuregui, E.J., et al., *Parallel mechanisms suppress cochlear bone remodeling to protect hearing.* Bone, 2016. **89**: p. 7-15.
86. Thorne, M., et al., *Cochlear fluid space dimensions for six species derived from reconstructions of three-dimensional magnetic resonance images.* Laryngoscope, 1999. **109**(10): p. 1661-8.
87. Rau, C., et al., *Quantitative X-ray tomography of the mouse cochlea.* PLoS One, 2012. **7**(4): p. e33568.

Figures

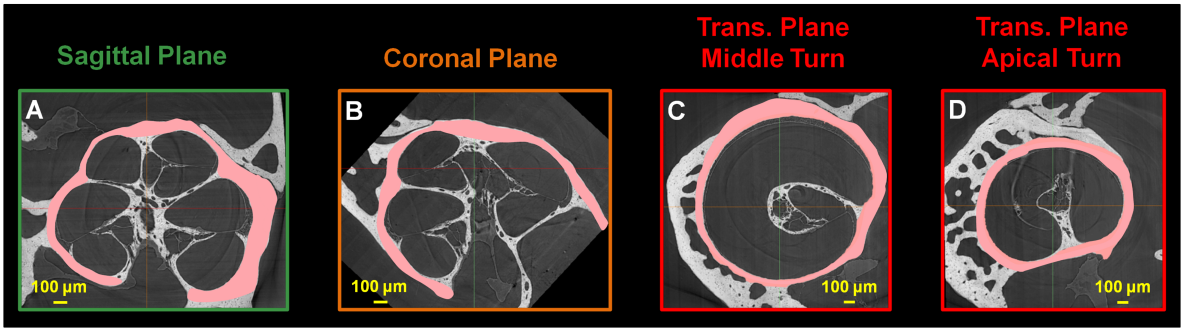

Fig. 1 Otic capsule cortical thickness A-D. Sagittal, coronal and transverse projections of one representative sample and otic capsule region of interest (pink areas) used for the evaluation of the average cortical thickness on each anatomical plane.

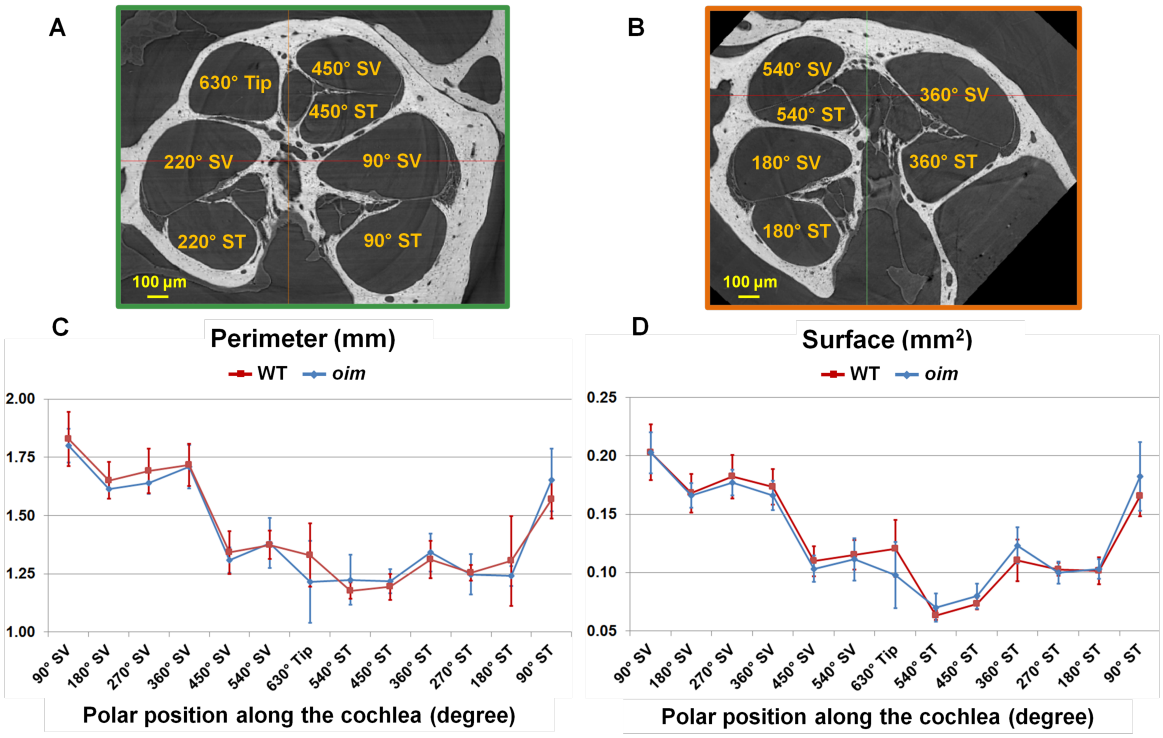

Fig. 2 Cochlear ducts surfaces and perimeters in WT and *oim* mice Cochlear ducts of a representative sample respectively in the **A.** sagittal and **B.** coronal plane. Surface and perimeter of the cochlear ducts are measured every 90 degrees along the cochlear spiral from the base to the apex. **C-D.** Perimeter and the surface of the fluid ducts (mean value ± standard deviation) along the cochlear spiral of the WT (red) and *oim* (blue) inner ear. SV = Scala Vestibuli, ST = Scala Tympani, and Tip = Fluid Scalae Tip. Despite scala vestibule and scala media are combined in the present study, our measurements are in agreement with previous studies on WT mice [86, 87].

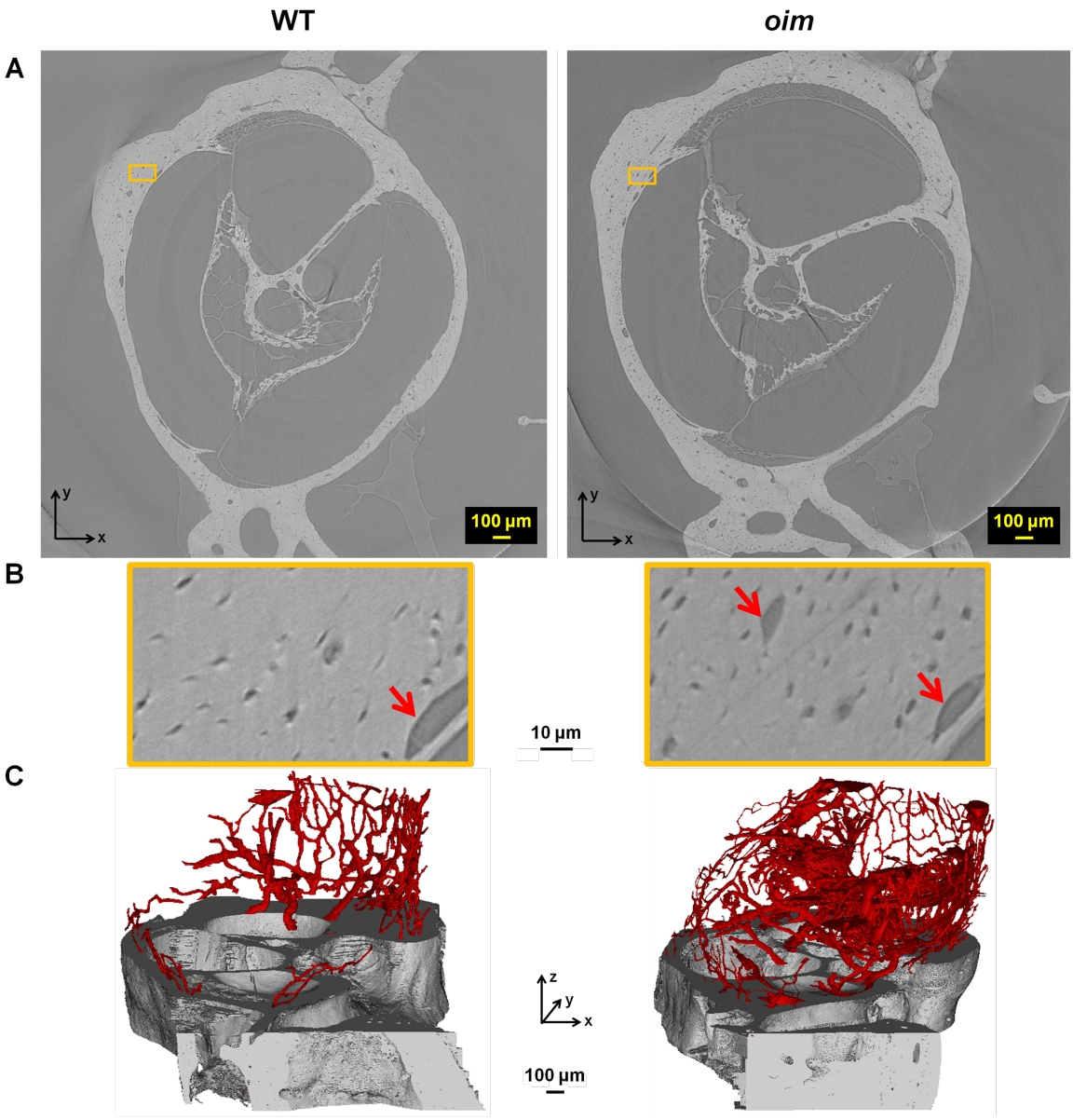

Fig. 3 Otic capsule intracortical porosity in WT and *oim* mice **A.** Synchrotron X-ray microtomographic slice and **B.** zoom-in of WT and *oim* representative otic capsule showing canals (red arrows) and intracortical lacunae (all the remaining voids in the bone tissue) **C.** 3D render of the canal network (red) within the WT and *oim* cochlea otic capsule (grey).

Tables

Otic capsule Morphological index	WT N = 6 bones	*oim* N = 6 bones	*p*-value WT vs. *oim*	Effect size (Cohen's *d*)
Oc.Th.cor (mm) thickness in coronal plane	0.07±0.01	0.08±0.01	<0.05	-0.92
Oc.Th.sag (mm) thickness in sagittal plane	0.09±0.01	0.08±0.01	n.s.	0.92
Oc.Th.tra.M (mm) thickness in transverse plane at middle turn	0.09±0.01	0.10±0.01	n.s.	-0.92
Oc.Th.tra.A (mm) thickness in transverse plane at apical turn	0.09±0.01	0.10±0.01	n.s.	-0.92
Oc.Le (mm) length	1.31±0.04	1.30 ±0.06	n.s.	0.18
Po.V/Ct.TV (%) porosity	5.46 ± 1.53	8.25 ± 0.83	<0.05	-2.09
N.Ca/Ct.TV (mm^{-3}) canal number density	5,352 ± 2,729	9,015 ± 3,610	<0.05	-1.11
Ca.V/Ct.TV (%) canal volume density	3.09 ± 0.95	5.75 ± 0.93	<0.05	-2.84
Ca.Conn.D (mm^{-3}) canal connectivity density	2,736 ± 1,410	4,624 ± 1,873	<0.05	-1.10
<Ca.V> ($10^3 \mu m^3$) mean canal volume	6.67 ± 2.22	7.28 ± 3.09	n.s.	-0.22
<Ca.D> (μm) mean canal diameter	12.25 ± 2.88	12.14 ± 3.24	n.s.	0.04
<Ca.Le> (μm) mean canal length	32.67 ± 38.90	29.94 ± 33.53	n.s.	0.08
N.Lc/Ct.TV (mm^{-3}) lacuna number density	144,252 ± 20,326	158,360 ± 26,372	n.s.	-0.60
Lc.V/Ct.TV (%) lacunae volume density	2.37 ± 0.67	2.50 ± 0.78	n.s.	-0.18
<Lc.V> (μm^3) mean lacuna volume	163.39 ± 103.20	156.89 ± 104.76	n.s.	0.06
<Lc.Eq> mean lacuna equancy	0.36 ± 0.14	0.38 ± 0.14	n.s.	-0.13
<Lc.El> mean lacuna elongation	0.20 ± 0.10	0.20 ± 0.10	n.s.	0.00
<Lc.Fl> mean lacuna flatness	0.53 ± 0.21	0.51 ± 0.20	n.s.	0.10
<Lc.ɵ> mean lacuna orientation	78.83 ± 37.97	79.68 ± 42.87	n.s.	-0.02

Table 1 Morphometric parameters characterizing the WT and *oim* otic capsule and their intracortical porosity (mean ± standard deviation).

Cochlear Fluid Scalae Morphological index	WT N = 6 bones	*oim* N = 6 bones	*p*-value WT vs. *oim*	Effect size (Cohen's *d*)
Sc.Fl.V(mm^3) total volume	1.29 ±0.03	1.26 ± 0.09	n.s.	0.41
Sc.Fl.Tip.V(mm^3) volume fluid scalae tip	0.03 ±0.01	0.02 ±0.01	n.s.	0.92
Sc.Fl.Sp.Le (mm) spiral length	7.77 ±0.31	7.60±0.15	n.s.	0.64
Sc.Fl.Pitch.tra.M (mm) spiral pitch at middle turn	0.31 ±0.02	0.32±0.02	n.s.	-0.46
Sc.Fl.Pitch.tra.A (mm) spiral pitch at apical turn	0.29 ±0.01	0.27 ±0.02	n.s.	1.17
Sc.Fl.corAxis.tra.M(mm) coronal axis at middle turn	1.55±0.02	1.52 ±0.04	n.s.	0.88
Sc.Fl.sagAxis.tra.M(mm) sagittal axis at middle turn	1.49 ±0.05	1.48±0.06	n.s.	0.17
Sc.Fl.corAxis.tra.A (mm) coronal axis at apical turn	1.21 ±0.04	1.18 ±0.03	n.s.	0.78
Sc.Fl.sagAxis.tra.A (mm) sagittal axis at apical turn	1.01 ±0.05	0.98 ±0.05	n.s.	0.55

Table 2 Morphometric parameters characterizing the fluid scalae of WT and *oim* cochlea (mean ± standard deviation).